Light-Driven Aggregation of Nanorobot Swarms for Precision Tumor Targeting in Manhattan-Geometry Vasculature

Luyao Zhang[1], Yue Sun[1,2(✉)], Dong Du[1], Yin Qing[1], and Yifan Chen[2]

[1] The School of Mechanical and Electrical Engineering, Chengdu University of Technology, Chengdu 610059, China
sunyuestc90@126.com

[2] The School of Life Science and Technology, University of Electronic Science and Technology of China, Chengdu 610000, China

Abstract. Early detection of tumors remains a critical challenge in oncology, necessitating the development of innovative and efficient detection techniques. This study proposes a novel approach for tumor targeting employing a swarm of nanorobots (NS) and their light-driven aggregation capabilities. By exploiting the interaction behavior of NS aggregation under light exposure, we aimed to improve tumor detection capabilities. The effectiveness of this approach was assessed through NS dispersion and search efficiency under various light conditions, including both periodic and aperiodic sources. The complex tumor microenvironment, characterized by a dense capillary network, leads to the formation of biological gradient fields (BGFs) within Manhattan-geometry vasculature (MGV). This research thoroughly investigates the behavior of NS within these specific environments, mimicking the navigational constraints imposed by MGV. Our findings validate the feasibility of utilizing light-driven NS aggregation for precise and efficient tumor targeting. The results establish a foundation for innovative tumor detection methodologies, emphasizing the significant potential of NS in clinical applications, especially within navigating MGV and responding to BGFs.

Keywords: Tumor targeting · Nanorobot swarms · Manhattan-geometry vasculature · Biological gradient fields · Light-driven aggregation

1 Introduction

Cancer constitutes a significant challenge in global health, being a major contributor to mortality worldwide. As Sung [1] reports, cancer accounts for nearly 10% of all human deaths annually, translating to almost 10 million lives. The high mortality rate is mainly attributed to the rapid proliferation and self-renewal

Y. Chen et al. (Eds.): BICT 2024, LNICST 592, pp. 161–172, 2025.
https://doi.org/10.1007/978-3-031-81599-7_16

capability of tumor cells, often leading to metastasis and the involvement of secondary organs. The development of tumor-supporting vasculature further facilitates the spread of cancer cells, complicating treatment efforts [2]. Early detection is crucial, with the potential to reduce up to 70% of cancer-related deaths globally [3]. Despite advances in medical imaging, early-stage cancers often go undetected until they progress to more advanced, less treatable stages.

The advent of nanotechnology has led to the development of nanorobot swarms (NS) composed of biocompatible materials, serving as both contrast agents and drug carriers [4]. These NS aim to enhance tumor site targeting and cancer cell binding, increasing lesion visibility. Traditional targeting methods, however, face limitations due to imaging capabilities and the non-selective nature of magnetic field controls, leading to errors in localization and steering [5].

An emerging solution is the autonomous in vivo computing framework, utilizing multi-agent system principles to enable NS to respond to biological gradient fields (BGFs) and navigate toward tumor sites autonomously. This approach, however, encounters challenges within the complex Manhattan-geometry Vasculature (MGV), where NS dispersion can impede effective navigation [6]. This study proposes light-driven NS aggregation as a novel strategy to overcome these obstacles [7]. Light stimulation can induce aggregation by incorporating light-sensitive molecules on NS surfaces, enabling precise control over NS behavior and enhancing their tumor-targeting efficacy [8].

This paper is structured as follows: Sect. 2 discusses the role of BGFs in NS navigation; Sect. 3 examines light-driven aggregation mechanisms; Sect. 4 compares the effectiveness of light-driven versus traditional search strategies; Sect. 5 concludes with future research directions in nanorobotics for cancer detection and treatment.

2 Tumor Micro-environment

2.1 BGFs in MGV

BGFs within the tumor microenvironment are pivotal for directing nanorobot swarms (NS) toward tumor sites. These fields are shaped by passive physical characteristics such as variations in nutrient concentration, oxygen levels, and metabolic by-products, leading to distinct growth states and metabolic traits in tumor cells. A notable manifestation of BGFs is the gradient distribution of vascular density within tumors, typically higher at the core due to increased demands for nutrients and oxygen [9], which induces blood vessel proliferation towards the tumor's core, creating a vascular density gradient field.

Compared to healthy tissues, tumor-induced heterogeneity constitutes BGFs, playing a vital role in guiding NS movements. As probes, NS navigates the vascular network, mapping internal biochemical gradients to an externally measurable objective function. The detection of tumors is signaled by global maxima

or minima within these gradients. The movement of NS is influenced by the network's architecture, with tumors generally developing at the network's extremities, where growth conditions are optimal [6] [10]. Research suggests the vascular structure near tumors resembles a two-dimensional mesh akin to Manhattan space, with BGFs propagation limited to vertical and horizontal directions.

This section elucidates the impact of BGFs on NS navigation within the challenging Manhattan-geometry Vasculature (MGV), highlighting the intricate dance between biological gradients and nanorobotics in pinpointing tumor locations.

2.2 Objective Function

In the absence of a universally recognized quantitative framework for BGFs, this research employs two Manhattan-like objective functions (1) and (2) to represent BGFs. The formulations of these functions are detailed as follows:

1) Diamond-Shaped Decay Function

$$F(x,y) = \begin{cases} 1 & \text{if } |x| + |y| \leq 0.8 \text{ and } (x,y) \in V, \\ [1 - 0.05(|x| + |y|)] & \text{if } |x| + |y| > 0.8 \text{ and } (x,y) \in V, \end{cases} \tag{1}$$

2) Composite Polynomial Decay Function

$$F(x,y) = \begin{cases} 1 \\ \quad \text{if } |x| + |y| \leq 0.8 \text{ and } (x,y) \in V, \\ \left[-0.0023(|x|^2 + |y|^2) - 0.0047|x||y| - 0.007|x|\right] \\ \quad \text{if } |x| + |y| > 0.8 \text{ and } (x,y) \in V. \end{cases} \tag{2}$$

The domain V represents the vascular network space around the tumor, which is the motion space constraint constraining the NS without detailed information about the blood vessels' diameter, the blood viscosity, and the blood pressure of the normal capillaries. Figure 1 illustrates the three-dimensional views and contour plots of two representative objective functions for BGFs. Panels (a) and (b) depict the Diamond-Shaped decay function and its corresponding contour plot, which represents an idealized form of BGF. This function features a highly symmetrical, peak-centered shape that simplifies the mathematical modeling of BGFs in an ideal scenario. Panels (c) and (d) show the Composite Polynomial decay function and its contours, representing a more conventional form of BGF. This function displays a less symmetrical, broader spread which might be more reflective of the typical variability seen in biological systems.

3 Light-Driven Aggregation of NS for in Vivo Computing

In the MGV systems framework, BGFs generate a rhombic field. The NS determine their movement direction based on the magnitude of the gradient they encounter. Groups on the same gradient line perceive no need for information

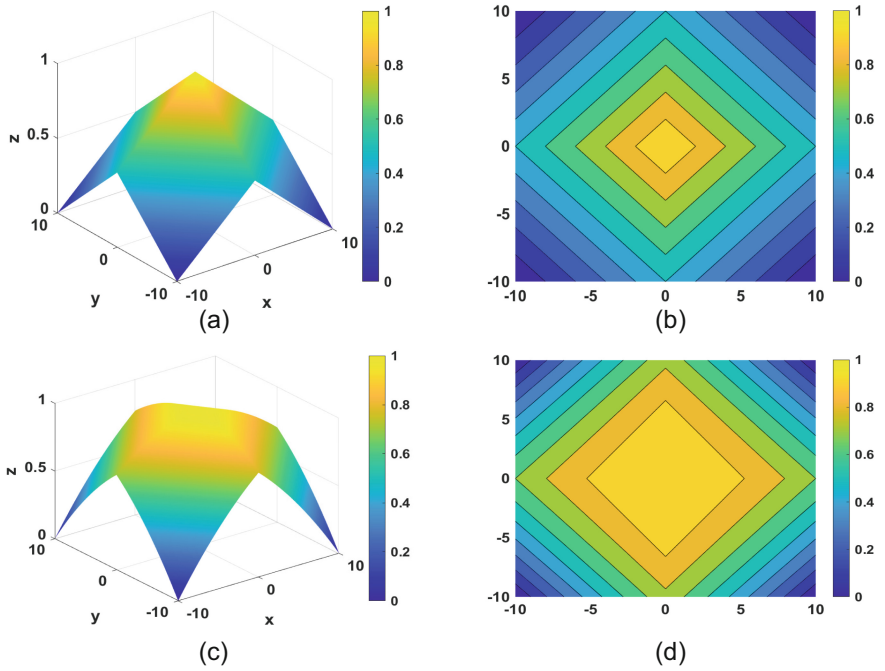

Fig. 1. Schematic diagrams of objective functions: (a) 3D view of the diamond-shaped decay function and (b) its contour plot; (c)3D view of the composite polynomial decay function and (d) its contour plot.

exchange, inhibiting their mutual convergence. As a result, the NS distribution naturally conforms to the gradient field's shape. Theoretically, the dispersion level of NS within a rhombic field is expected to surpass that within an Euclidean space due to the field's inherent linearity. We advocate for a light-triggered aggregation system to address the reduced search efficiency stemming from NS's excessive dispersion. The aggregation mechanism of nanorobots and their motion dynamics in response to BGFs are elucidated in the following text.

3.1 Light-Driven Aggregation

NS are capable of autonomous motion or directed migration under the influence of localized or extensive chemical gradients and external stimuli, including light, magnetic fields, electric fields, thermal gradients, acoustic waves, and fluidic forces [11]. NS may coalesce into functional assemblies or complex structures during these processes through inter-particle or particle-surface interactions. As a pivotal external actuator, light provides significant advantages for remote manipulation and precise spatiotemporal regulation. Additionally, due to its finely tunable energy output and directionality, light is extensively utilized to control

nanorobots' operational states, velocity, and directional guidance, making it an essential tool in nanorobotics [12].

Although the NS exhibit slight structural variations, they adhere to some fundamental principles during their formation processes. In the swarm, the interactions among individual nanorobots are predominantly governed by dynamic long-range attractive forces and short-range repulsive forces. The long-range attractions facilitate the clustering of nanorobots, enhancing collective behavior, whereas the short-range repulsions are critical for preventing inter-robotic collisions, thereby maintaining the structural integrity of the swarm. [13]. The formation of NS is contingent upon achieving a sufficient balance between the attractive and repulsive forces among the nanorobots.

We refined the fundamental model [14] to depict aggregation dynamics in collective behaviors. Within this model, the state of each nanorobot, denoted as $\boldsymbol{x}_i(t) = \boldsymbol{x}(\delta_i(t))$, within a localized region of the simulation domain V, and its interactions with neighboring units (represented by the set N_i), are updated at any given moment $t \in T$ based on a local rule Ψ.

$$\boldsymbol{x}_i(t+\epsilon) = \psi\left(\boldsymbol{x}_i(t), \boldsymbol{x}_{N_i}(t)\right) \tag{3}$$

In this context, $\boldsymbol{x}_{N_i}(t) = \{\boldsymbol{x}_j(t) \mid \delta_j \in N_i\}$ represents the states of neighboring nanorobots i at time t, with ϵ indicating the minimal time increment. Interaction rule localization is achieved by restricting N_i, which is the set of nanorobots neighboring δ_i, defined as a subset consisting of nanorobots with states proximal to δ_i.

$$N_i = \{\delta_j \mid d(\boldsymbol{x}_i(t), \boldsymbol{x}_j(t)) \leq \Delta\} \tag{4}$$

where $d(\cdot,\cdot)$ denotes the distance metric, and Δ serves as a parameter that specifies the interaction radius. The set N_i evolves temporally in response to Eq. 4, reflecting the dynamic states of the nanorobots.

The convergence evolution process refers to a system's overall pattern in which the characteristics of nanorobots within the state space gradually become uniform. This indicates that all nanorobots' states converge towards a global average state. The complexity of this process lies in the fact that each nanorobot interacts only with its nearby neighbors, thereby lacking the ability to ascertain the exact positions of all nanorobots within the state space. Each nanorobot can only acquire information about relative positions at any given moment through interactions with its neighbors. For each nanorobot δ_i, the relative positions of its neighbors in the state space are defined as:

$$\boldsymbol{r}_{ij}(t) = \boldsymbol{x}_j(t) - \boldsymbol{x}_i(t) \tag{5}$$

With this information, nanorobot δ_i can only estimate the locally averaged state of the swarm as it evolves.

$$\bar{\boldsymbol{x}}_i(t) = \boldsymbol{x}_i(t) + \frac{1}{|N_i|+1} \sum_{\delta_j \in N_i} \boldsymbol{r}_{ij}(t) \tag{6}$$

The $|N_i| + 1$ is used to deal with the case with $|N_i| = 0$.

With continuous innovation in mechanisms and control strategies, the light-driven aggregation of NS, characterized by easy operation, low cost, and widespread applicability, can be applied to early-stage tumor targeting.

3.2 The NS Motion Dynamics

The Fig. 2 presents a schematic flowchart describing the process of nanorobot operation for tumor detection, emphasizing the light-driven aggregation mechanism. The steps covered in the framework include:

- **Initialization:** We initiate with N nanorobots, all injected nanorobots experience the BGFs as η_1, η_2, η_3, ..., η_N in the domain V where $\eta_1 = f(x_1)$, $\eta_2 = f(x_2)$, $\eta_3 = f(x_3)$, ..., $\eta_N = f(x_N)$.

$$\Delta\eta = \eta_i - \eta_n \tag{7}$$

  Here, η_i and η_n represent the gradients sensed by the nanorobots and their neighbors, respectively. Equation (7) describes the scenario of a search space under ideal conditions. The natural environment invariably introduces distortions from nonidealities, including nanorobots' learning errors and distortions during the transmission process. Consequently, we introduce a random error into Eq. (7) following a normal distribution:

$$\eta_\epsilon = \Delta\eta + \chi(\mu, \sigma) \tag{8}$$

  Here, η_ϵ represents the difference in the distorted BGFs value, while χ refers to noise with a mean of zero ($\mu = 0$) and a standard deviation σ for simplified calculations.
- **Neighbor Selection:** We propose that the neighbor selection criterion should allow for a dynamic K, transitioning from a fixed to a variable number. This would enable more effective cooperation within the NS based on the influence range of the push-pull effect. Each neighbor of a nanorobot will exert a push or pull on it based on the differences in the sensed BGFs values.
- **Light-driven Aggregation:** After interacting with K neighbors, each computational agent determines whether it is "attracted" or "repelled" by its neighbors, thereby generating a clustering effect. Neighbors experiencing significant changes in BGFs exert a greater attraction, causing surrounding computational agents to move closer and vice versa. Upon reaching the luminescence cycle, the external system activates a light source, inducing a clustered drive force in the NS, causing convergence, and modifying the influence of each neighbor on the computational agent. Thus, the interaction between neighboring nanorobots and the computational agent during the illumination period is described by:

$$M_L = \begin{cases} \frac{\eta_\epsilon}{[\Delta d/d_{ref}]^l} + E_l e^{-\triangle d}, \text{ K neighbors} \\ 0, \text{ other nanorobots} \end{cases} \tag{9}$$

Here, M_L represents the interaction effect on a nanorobot from its neighbor. $\Delta\eta$ denotes the difference in sensed BGFs values, Δd is the Manhattan distance between a nanorobot and its neighbor, d_{ref} serves as a normalization factor and l is the path-loss exponent. E_l denotes the driving force among NS post-light source activation, with its magnitude dependent on the light source's physical characteristics or power. Path loss in propagation, influenced by the distance between the computing agent and its neighbors, also occurs due to the MGV environment.

According to Eq. (5), for each nanorobot, the relative coordinates between it and its neighbors are represented as $\boldsymbol{r}_{ij}(t)$. Equation (9) illustrates the interaction behavior of a single nanorobot-neighbor pair. The nanorobot acts with its surrounding K neighbors. The overall magnitude of the interactions with the resultant direction is calculated as

$$\boldsymbol{S} = \sum_{i=1}^{K} M_L^{(i)} \boldsymbol{r}_{ij}(t) \tag{10}$$

The $\boldsymbol{S}$ represents the sum of the repulsive and attractive forces induced by K neighbors, which determines the direction of the next movement of the computing agent.

– **Migration:** After monitoring the environment and sharing the tumor-induced BGFs with neighbors, the next step is to facilitate the migration of the NS to a globally optimal location, whose position update follows the following formula:

$$\boldsymbol{x}_{i+1} = \boldsymbol{x}_i + \gamma \boldsymbol{S} \tag{11}$$

Here, $\boldsymbol{x}_i$ represents the current position, while $\boldsymbol{x}_{i+1}$ denotes the next position of the nanorobots. The step size γ is a crucial factor influencing determining the subsequent location. Note that γ is a critical parameter determined by various factors, including the nanorobots' material properties, shape and size, initial conditions, external environment, propulsion mechanisms, and motion algorithms.

4 Performance Analysis

4.1 Simulation Settings

Numerical simulations are conducted in MATLAB to evaluate the performance of the periodic light-driven autonomous search strategy. The two different objective functions proposed above represent in vivo tumor-induced BGFs, where the search region is $-10\,\text{mm} \leq x, y \leq 10\,\text{mm}$, the injection areas for the nanorobots are $-10\,\text{mm} \leq x, y \leq -9\,\text{mm}$. The MGV environment was simulated with a grid model spaced at 0.01 mm. The other simulation parameter settings are given in Table 1, and the parameters of this simulation were carried out according to the data in the table unless otherwise stated. The NS cannot move forward in the

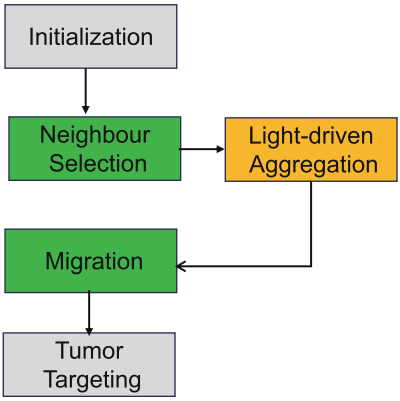

Fig. 2. Flowchart of computation framework.

opposite direction of the blood flow direction, meaning they can only update their position information in two directions (up or to the right), and both directions have the same probability. The NS follows the steps of the search strategy, and beyond the search time, the nanorobot is considered to have lost its functionality. When the nanorobots reach a tumor area with a radius of 0.8 mm, they are considered to have successfully searched for a tumor.

Table 1. Simulation Parameter Settings

Parameter name	numerical value
Blood flow rate (mm/s)	0.05
Number of nanorobots	25
Initial step (mm)	0.5
Dynamic Neighbor Sensing Range(mm)	0.6
Light source period(s)	5
Maximum search time(s)	250
Constant driving force	0.1

To evaluate the performance of the periodic light-driven autonomous search strategy, it is compared with the search strategy without light-driven and two performance metrics are given:

– **Dispersion:** Calculated from two means, first calculate the distance between a single nanorobot and the geometric center of gravity of the population at each iteration in a single simulation run to obtain the standard deviation of the distance. It is assumed that the distances of N nanorobots from the geometric center of the population in a single iteration are expressed

as $d_1, d_2, ..., d_N$, these distances give the standard deviation of distances for evaluating the dispersion of the current group d_{SD}:

$$d_{SD} = \sqrt{\frac{\sum_{i=1}^{N}(d_i - \bar{d})^2}{N-1}} \tag{12}$$

From a complete search process, assume that the number of iterations is C, get the average value of $d_{SD}^{(1)}...d_{SD}^{(c)}$ is $\overline{d_{SD}}$:

$$\overline{d_{SD}} = \frac{\sum_{c=1}^{C} d_{SD}^{(c)}}{C} \tag{13}$$

Finally, the multiple obtained from the total number of simulations were counted $\overline{d_{SD}}$. The average dispersion measure, denoted as $\overline{D}$, is calculated to represent the mean of the standard deviation of distances $\overline{d_{SD}}$ obtained from a series of independent simulation runs. Mathematically, $\overline{D}$ is expressed as:

$$\overline{D} = \frac{1}{M}\sum_{m=1}^{M} \overline{d_{SD}^{(m)}} \tag{14}$$

where M represents the total number of independent simulations conducted, and $\overline{d_{SD}^{(m)}}$ denotes the computed value of $\overline{d_{SD}}$ from the mth simulation. This measure provides insight into the consistency and variability of the NS dispersion across different simulation scenarios. A lower value of $\overline{D}$ indicates a more consistent and tight spatial distribution of the nanorobot population across multiple simulations, suggesting that the NS exhibits a stable aggregation behavior under varying conditions. Conversely, a higher value of $\overline{D}$ reflects greater variability in the dispersion of the population, indicating that the NS's spatial distribution is more variable across different simulations.

– **Search efficiency:** The search efficiency of the NS in locating tumors is quantitatively evaluated by calculating the mean ratio of the number of NS that successfully locate the tumor to the total number of NS injected across multiple simulation runs. This efficiency is mathematically represented as follows:

$$\text{Search Efficiency} = \frac{1}{M}\sum_{m=1}^{M}\left(\frac{N_{\text{successful},m}}{N_{\text{total},m}}\right) \tag{15}$$

where M denotes the total number of simulation runs, $N_{\text{successful},m}$ is the number of NS that successfully locate the tumor in the mth simulation, and $N_{\text{total},m}$ is the total number of NS injected in the mth simulation. A higher search efficiency indicates a greater proportion of NS reaching the tumors, thereby reflecting the accuracy of the employed strategy.

4.2 Simulation Results

Figure 3 illustrates the trajectories of our search strategy powered by light exposure in the diamond-shaped decay function, juxtaposed with a control strategy

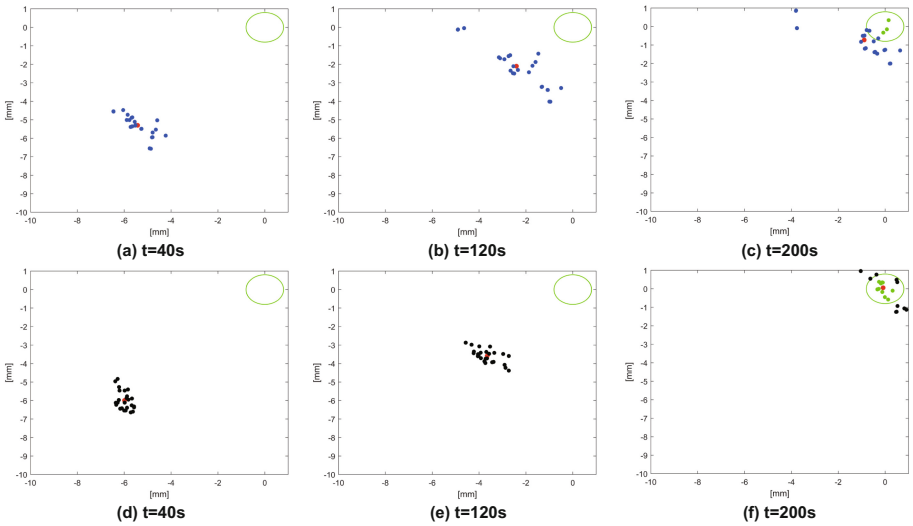

Fig. 3. Trajectory map of autonomous NS without light (a-c) and trajectory map of autonomous NS based on light-driven aggregation(d-f).

that operates without a light source under identical simulation parameters and timeframe. In these diagrams, red dots signify the centroid of the population geometry, blue and black dots denote the NS within each respective strategy, and the green circle marks the tumor's center. The diagrams reveal that the NS exhibit a significantly higher degree of aggregation when subjected to the periodic light source compared to their counterparts in the non-light-driven approach. Furthermore, more NS successfully reach and accumulate in the tumor area, facilitated by the enhanced permeability and retention effect upon contact with the tumor's center. This enhanced aggregation and tumor-targeting efficiency under light exposure is similarly observed in the composite polynomial decay function context. The histogram in Fig. 4 compares the dispersion and search efficiency of an autonomous search strategy assisted by a light source versus a non-light-assisted approach applied to an objective function characterized by the Manhattan distribution. The graph shows that the NS exhibits greater dispersion without a light source. In contrast, introducing the light source as a driving force for aggregation significantly reduces dispersion. The final search efficiency is also improved. Low dispersion indicates a high degree of aggregation between NS, which enhances adhesion between nanorobots and reduces the number of nanorobots unable to cooperate due to excessive distance between them. This also minimizes the likelihood of nanorobots being carried by the bloodstream into incorrect vascular branches, thereby increasing the number of nanorobots that successfully reach the tumor area.

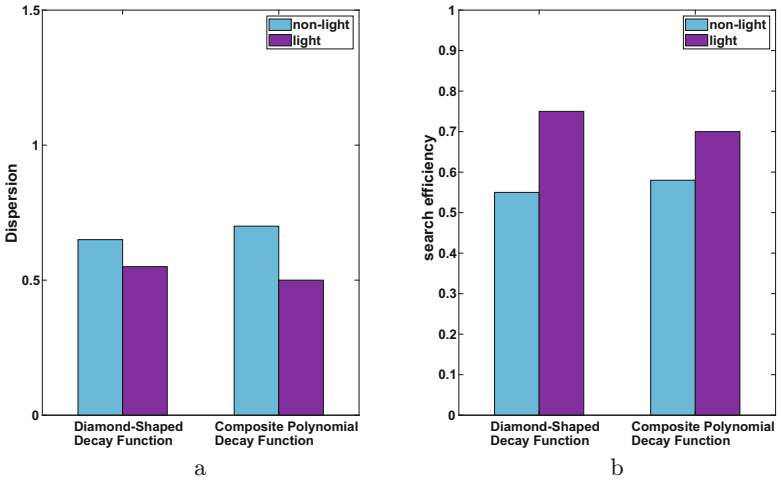

Fig. 4. The autonomous search strategies under light and without light sources: (a) Dispersion histograms for two types of objective functions. (b)Search efficiency histograms for two types of objective functions.

5 Conclusion

In this study, we introduced an innovative search strategy that leverages periodic light-driven aggregation to enhance autonomous in vivo computing. By employing a light source from an external system, we significantly bolstered NS aggregation capabilities during the tumor search process within the intricate MGV. Our simulation experiments underscored a marked improvement in search efficiency when the light-driven mechanism was implemented, highlighting the strategy's effectiveness over traditional methods that do not utilize such a driving force. This work could inspire further exploration into light-driven mechanisms for other applications in nanotechnology and swarm intelligence. Additionally, investigating the integration of this strategy with other stimuli-responsive systems may uncover new synergies, further expanding the potential impact of our findings.

Funding Information. This work is supported by the National Natural Science Foundation of China (Grants No. 62301088).

References

1. Sung, H., et al.: Global cancer statistics 2020: GLOBOCAN estimates of incidence and mortality worldwide for 36 cancers in 185 countries. CA: Cancer J. Clin. **71**(3), 209–249 (2021)
2. Schaaf, M.B., Garg, A.D., Agostinis, P.: Defining the role of the tumor vasculature in antitumor immunity and immunotherapy. Cell Death Dis. **9**(2), 115 (2018)

3. Smith, R.A., et al.: Cancer screening in the united states, 2019: A review of current American cancer society guidelines and current issues in cancer screening. CA: Cancer J. Clin. **69**(3), 184—210 (2019). https://doi.org/10.3322/caac.21557
4. Von Maltzahn, G., et al.: Nanoparticles that communicate in vivo to amplify Tumour targeting. Nat. Mater. **10**(7), 545–552 (2011)
5. Chen, Y., Ali, M., Shi, S., Cheang, U.K.: Biosensing-by-learning direct targeting strategy for enhanced tumor sensitization. IEEE Trans. Nanobiosci. **18**(3), 498–509 (2019)
6. Sun, Y., Qing, Y., Chen, Y.: In vivo computing for smart tumor targeting in taxicab-geometry vasculature. IEEE Trans. Nanobiosci. **21**(3), 445–453 (2022). https://doi.org/10.1109/TNB.2022.3149960
7. Ragazzon, G., Baroncini, M., Silvi, S., Venturi, M., Credi, A.: Light-powered autonomous and directional molecular motion of a dissipative self-assembling system. Nat. Nanotechnol. **10**(1), 70–75 (2015)
8. Pan, P., Svirskis, D., Rees, S.W., Barker, D., Waterhouse, G.I., Wu, Z.: Photosensitive drug delivery systems for cancer therapy: mechanisms and applications. J. Control. Release **338**, 446–461 (2021)
9. Sun, Y., Bian, H., Chen, Y.: A photolysis-assist molecular communication for tumor biosensing. Sensors **22**(7), 2495 (2022)
10. Baish, J.W., Jain, R.K.: Fractals and cancer. Can. Res. **60**(14), 3683–3688 (2000)
11. Law, J., et al.: Microrobotic swarms for selective embolization. Sci. Adv. **8**(29), eabm5752 (2022)
12. Zhang, J., Guo, J., Mou, F., Guan, J.: Light-controlled swarming and assembly of colloidal particles. Micromachines **9**(2), 88 (2018)
13. Grzybowski, B.A., Fitzner, K., Paczesny, J., Granick, S.: From dynamic self-assembly to networked chemical systems. Chem. Soc. Rev. **46**(18), 5647–5678 (2017)
14. Tian, Y., Xu, Y., Sun, P.: Laplacian dynamics of convergent and divergent collective behaviors. J. Phys. Complex. **4**(2), 025013 (2023)